University of Glasgow
DEPARTMENT OF
AEROSPACE
ENGINEERING

Modification and Analysis of Hibrom / Genisa Inverse Simulation

Sharon Moir

Dr. Douglas G. Thomson

Internal Report No. 9827, September 1998

Modification and Analysis of Hibrom / Genisa Inverse Simulation

Sharon Moir

Dr. Douglas G. Thomson

Internal Report No. 9827, September 1998

Abstract

The individual blade rotor model Hibrom has been extended to include the dynamics of an engine and rotorspeed governor. In order to incorporate the new model within the inverse simulation algorithm Genisa, the control application interval must be varied with each time step to match the periodicity of the main rotor. Modifications have been made to Genisa to achieve this. Verification of the revised algorithm is demonstrated and its limitations are discussed.

Contents

Nomenclature

$\boldsymbol{A}$, $\boldsymbol{B}$	system and control matrices	(units vary)
e	hinge offset	
$\underline{F}(\underline{x},\underline{u},t)$	nonlinear vector function of motion	
g	acceleration due to gravity	(m / s^2)
h	maximum manoeuvre height	(m)
I_{xx}, I_{yy}, I_{zz}	aircraft moments of inertia referred to body axes	(kg m^2)
I_{xz}	aircraft product of inertia	(kg m^2)
I_β	blade flapping inertia	(kg m^2)
I_R	effective inertia of the main rotor	(kg m^2)
k	current solution time point	
K_β	blade hinge spring stiffness	(m / rad)
K_{e1}, K_{e2}, K_3	engine model gains	
L, M, N	components of external moment on aircraft	(N m)
m	aircraft mass	(kg)
$\overline{m}$	blade mass per unit span	(kg / m)
M_β	blade mass moment	(kg m)
nbl	number of rotor blades	
n_{pts}	number of points in inverse simulation / manoeuvre	
p, q, r	helicopter angular velocity components	(rad / s)
Q_E	engine torque	(N m)
Q_{Emax}	maximum engine torque	(N m)
Q_R	main rotor torque	(N m)
Q_{TR}	tail rotor torque	(N m)
Q_{tr}	transmission torque	(N m)
r	distance from main rotor hub to point on blade	(m)
R	main rotor radius	(m)
t	time	(sec)
T	Time constant of a first order system	(sec)
t_k	time point in inverse simulation / manoeuvre definition	
t_m	time taken to complete a manoeuvre	(sec)
$\underline{\boldsymbol{u}}$	control vector	
u, v, w	translational velocity components	(m / s)
V_f	aircraft flight velocity	(m / s)
$\boldsymbol{W}$	matrix of system eigenvectors	
$\underline{\boldsymbol{x}}$	state vector	(units vary)
$\underline{\boldsymbol{x}}_0$	initial state vector	(units vary)

X, Y, Z	components of external force on aircraft	(N)
X_u, etc.	stability and control derivatives	(units vary)
$\underline{x}_e$	trim state vector	(units vary)
x_e, y_e, z_e	displacements relative to an earth fixed inertial frame	(m)
$\underline{y}$	output vector	(units vary)
$\underline{y}_{des}$	desired output vector	(units vary)
β	blade flap angle	(rad)
Δt	inverse simulation / manoeuvre discretisation interval	(sec)
δx	state perturbation size	
δu	control perturbation size	
ϕ, θ, ψ	aircraft attitude angles	(rad)
λ	linear system eigenvalues	(1 / s)
λ_β	blade flapping frequency	(1 / s)
θ_0	main rotor collective pitch angle	(rad)
θ_{1s}, θ_{1c}	main rotor longitudinal and lateral cyclic pitch angles	(rad)
θ_{0tr}	tail rotor collective pitch angle	(rad)
ρ	local air density	(kg / m^3)
τ_{e1}, τ_{e2}, τ_{e3}	engine time constants	(sec)
ω_f	fuel flow variable	
Ω	main rotorspeed	(rad / s)
Ω_i	idling rotorspeed	(rad / s)
ψ_{azi}	blade azimuth angle	(rad)

1. Introduction

In recent years there has been growing interest in the concept of inverse simulation[1,2]. This is a technique whereby the control inputs required for a modelled vehicle to perform a specified manoeuvre are determined. The application of this type of simulation to helicopter flight dynamics studies has been particularly fruitful and The Department of Aerospace Engineering at Glasgow University has maintained a lead in this area for many years. The studies conducted at Glasgow to date range from the investigation of piloting strategies for offshore operations[3] to the assessment of helicopter handling qualities and pilot workload[4,5].

The first inverse simulation developed at Glasgow, Helinv[6], was based around a nonlinear model, HGS, which uses an actuator disc representation of a single main and tail rotor helicopter. The solution algorithm employs numerical differentiation. Helinv has proved to be a valuable tool with many varied applications; however it suffers from being model-specific and from the instabilities associated with numerical differentiation.

These problems were overcome with the development of a more stable integration based inverse algorithm, Genisa, which lends itself to any model[7,8]. A more sophisticated individual blade model, Hibrom, could then be incorporated which signified a major advancement and has taken inverse simulation into a new area of applicability. For example, with this type of rotor model, it is possible to simulate flight near the edges of the helicopter's flight envelope. However, in achieving this step, the number of modelling features were restricted to a minimum with a view to augmentation at some later date.

This report describes modifications which have been made to allow the rotorspeed degree of freedom to be added to the mathematical model. This reflects the physical situation more closely, where changes in blade pitch lead to changes in torque demand and a continuous variation in rotorspeed. Hibrom does not model this effect, assuming constant rotorspeed for simplicity. A brief summary of the main features of the existing model, Hibrom, will be followed by an outline of the engine model to be incorporated and a discussion of the blade flapping model. Linearisation of the enhanced individual blade model will then be described and the dynamic characteristics of the fuselage modes discussed analytically.

The addition of rotorspeed degree of freedom to the model has implications for the solution algorithm, Genisa, which are discussed in the second part of the report. Verification of a suitably revised algorithm is demonstrated for the Westland Lynx helicopter flying a hurdlehop manoeuvre and restrictions on the control application interval are discussed. The necessity for these restrictions is then explained with reference to the dynamic characteristics of different modes of the helicopter.

2. Helicopter Individual Blade Rotor Model : Hibrom

2.1 Review of Hibrom v.1

Hibrom v.1 (version 1) is an individual blade model of the main rotor based on blade element theory which, when combined with available tail rotor, fuselage, tailplane and fin models, can be used to simulate a single main and tail rotor helicopter such as the Westland Lynx or Aerospatiale Puma. This type of rotor model offers several advantages over the established disc model representation. For example, the dynamics and geometry of each blade can be modelled separately and empirical blade aerodynamic data are easily incorporated. More fundamental, however, is the fact that the periodic nature of the rotor forcing and blade dynamics is captured by an individual blade model.

Hibrom v.1 represents the first attempt at applying an individual blade model to inverse simulation. As such, it is based on many simplifying assumptions, most of which are re-stated here:

(i) ideal atmospheric conditions,
(ii) inertial forces (other than centrifugal) neglected,
(iii) Peters and HaQuang dynamic inflow model,
(iv) constant rotorspeed,
(v) fully rigid rotor blades,
(vi) lead / lag dynamics not modelled,
(vii) torsional rigidity,
(viii) full flapping dynamics,
(iv) look-up tables for 2D blade aerodynamic data (as functions of angle of attack and Mach number), incorporating steady aerodynamics only (no modelling of the dynamic stall phenomenon),

(v) blade flapping modelled by an effective flap hinge offset,

(vi) blade geometry consisting of a simple linear twist and constant chord (with root cut-out) for all blades.

2.2 Modifications to Hibrom

Some changes have been made to the Hibrom v.1 model which will now be described. The modified version of Hibrom will from here on be referred to as Hibrom v.2.

i) Inclusion of an Engine Model

In Hibrom v.1, the simplifying assumption was made that rotorspeed remains constant throughout any manoeuvre at a value corresponding to zero engine torque. In reality, changes in torque demand will result in a continuously varying rotorspeed which is sensed by an engine governor. The governor then attempts to redress the imbalance by demanding a suitable change in fuel flow, thereby increasing or decreasing the engine torque output as required. Naturally there is a lag between the rotorspeed change and the resulting torque change and hence the rotorspeed is a degree of freedom within the system. An attempt has been made to implement an engine and rotorspeed model within Hibrom v.2. The model is essentially that given by Padfield[9] and is described briefly here.

Rotorspeed, Ω, is related to the engine torque output, Q_E, by the equation:

$$\dot{\Omega} = \left(\frac{1}{I_R}\right)\left(Q_E - Q_R - Q_{TR} - Q_{tr}\right) + \dot{r}; \qquad (2.1)$$

where Q_R, Q_{TR} and $Q_{tr} = I_{tr}\dot{\Omega}$ are the torques required to drive the main rotor, tail rotor and transmission system respectively; I_R is the effective inertia of the rotor system, given by the sum of the inertias of the individual blades, $I_R = n_{bl} I_\beta$, and r is the fuselage yaw rate.

The engine and rotorspeed governor is modelled by two first order systems with feedback loops. Firstly, the governor senses a change in rotorspeed and demands a fuel flow change, $\Delta\omega_f$, to compensate. This is represented by a single lag, with transfer function:

$$\frac{\Delta\omega_f}{\Delta\Omega} = \frac{K_{e1}}{1+\tau_{e1}s} \tag{2.2}$$

The engine torque response to this fuel flow change can be written as a lead/lag element of the form:

$$\frac{\Delta Q_E}{\Delta\omega_f} = K_{e2}\left(\frac{1+\tau_{e2}s}{1+\tau_{e3}s}\right) \tag{2.3}$$

The overall engine torque response to a change in rotorspeed is then given by the 2nd order, nonlinear differential function:

$$\ddot{Q}_E = \frac{1}{\tau_{e1}\tau_{e3}}\left[-(\tau_{e1}+\tau_{e3})\dot{Q}_E - Q_E + K_3\left(\Omega - \Omega_i + \tau_{e2}\dot{\Omega}\right)\right] \tag{2.4}$$

where Ω_i is the idling rotorspeed, corresponding to approximately zero engine torque, and $K_3 = K_{e1}K_{e2}$ is the system gain. The lead and lag time 'constants', τ_{e2} and τ_{e3}, are in fact functions of engine torque and a linear variation is adopted between flight idle and maximum power:

$$\tau_{e2} = \tau_{20} + \tau_{21}\left(\frac{Q_E}{Q_{E\,max}}\right)$$

$$\tau_{e3} = \tau_{30} + \tau_{31}\left(\frac{Q_E}{Q_{E\,max}}\right) \tag{2.5}$$

Equations (2.1) and (2.4) are now included in the main rotor model, resulting in three additional degrees of freedom corresponding to Ω, Q_E and $\dot{Q}_E$.

ii) Blade Flapping Model

Teetering, articulated and bearingless rotor arrangements can all be modelled by some combination of offset hinge and spring, provided the correct flapping frequency, λ_β, is maintained in accordance with the relationship given by Young[10]:

$$\lambda_\beta{}^2 = 1 + \frac{K_\beta}{I_\beta\Omega^2} + \frac{eRM_\beta}{I_\beta}; \tag{2.6}$$

where Ω is the rotorspeed, K_β is the spring stiffness and e is the hinge offset, expressed as a fraction of the rotor radius, R. The blade flapping inertia, I_β, and blade mass moment, M_β, are functions of the hinge offset, given by

$$I_\beta = \int_{eR}^{R} (r - eR)^2 \overline{m}\, dr \tag{2.7}$$

and

$$M_\beta = \int_{eR}^{R} (r - eR) \overline{m}\, dr; \tag{2.8}$$

where $\overline{m}$ is the blade mass distribution.

The Westland Lynx is a hingeless rotor helicopter which achieves both flap and lead-lag motion through elastic bending. In this arrangement, blade pitch control is effected through a bearing near the blade root. Hingeless or bearingless rotors have the advantage of a mechanically simpler hub and are capable of producing hub moments which are about four times those generated by a typical articulated rotor. This results in increased control sensitivity and damping, at the expense of greater sensitivity to external disturbances.

Hibrom v.1 models blade flapping using an effective hinge offset with zero spring stiffness; a semi-rigid rotor such as the Lynx is thus represented by a large hinge offset while a fully-articulated rotor requires only a relatively small value. The actuator disc model, HGS[11], uses a so-called centre spring equivalent rotor model, where it is assumed that all blade flapping occurs about a centrally sprung hinge with a restoring moment proportional to the flapping angle, β, through an equivalent spring stiffness, $K\beta$. The individual blade model RASCAL[12], also developed at Glasgow University, varies its representation of blade flapping to suit the type of helicopter being modelled. A hingeless rotor helicopter such as the Lynx is modelled by a centre spring while an offset hinge representation is preferred for fully articulated rotors such as that on the Aerospatiale Puma. Values of spring stiffnesses and equivalent hinge offsets are given in Table 1 for the Lynx and Puma.

Helicopter	Spring Stiffness K_β (Nm/rad) (Centre-Spring Model)	Equivalent Hinge Offset e
Lynx	166 352	0.274
Puma	48 149	0.0387

Table 1: Spring Stiffnesses and Equivalent Hinge Offsets for the Lynx and Puma

It is debatable which model of blade flapping is the most appropriate for flight simulation of a hingeless rotor helicopter. Padfield[13] advocates the use of a centre-spring model due to its simplicity and its ability to preserve the correct phasing between control and flapping and between flapping and hub moment. This is in spite of its poor approximation to the blade shape in deformation. Hibrom v.2 has been modified to encompass a centre-spring blade flapping model for hingeless rotor helicopters.

iii) Development of a Linearised Version of Hibrom

The general aim of simulation modelling is to approach physical realism, subject to practical constraints, in order to predict the behaviour of a dynamic system. In the field of helicopter flight dynamics, models of ever-increasing complexity and hence fidelity are becoming possible with advances in computing technology. Despite this, a good physical understanding of helicopter flight behaviour can only be derived by recourse to conventional analytical theory, requiring simple approximations to be made. The theory of linear dynamic systems is applied to Hibrom v.2 and used to study the stability and control characteristics of a Westland Lynx in chapter 3. First of all, linearisation of the Hibrom v.2 model will be described.

The nonlinear equations of motion are given by

$$\dot{\underline{x}} = \underline{F}(\underline{x}, \underline{u}, t) \tag{2.9}$$

where $\underline{x}$, $\underline{u}$ are the system state and control vectors respectively and t represents time. For an 11th order system consisting of fuselage and engine states, the state vector is

$$\underline{x} = \left(u, w, q, \theta, v, p, \phi, r, \Omega, \dot{Q}_E, Q_E\right)^T$$

where u, v, w are the translational velocity components along the three orthogonal directions of the body-fixed axis system; p, q, r are the corresponding angular velocities and θ, ϕ are Euler angles defining the orientation of the body axes relative to the earth. The third Euler angle, heading (ψ), is not included since the direction of flight in the horizontal plane will have no effect on the aircraft dynamic behaviour.

The control vector includes main rotor collective, longitudinal cyclic, lateral cyclic and tail rotor collective

$$\underline{u} = \left(\theta_0, \theta_{1s}, \theta_{1c}, \theta_{0tr}\right)^T$$

In appendix 1, the nonlinear equations (2.9) may be referred to in expanded form.

Linearisation of the equations of motion is achieved by means of small disturbance theory. This theory is based on the idea that, in disturbed flight, the aircraft's motion may be regarded as a perturbation from the reference trim condition. Hence, each state and control can be written as the sum of a steady trim component and a small perturbation from trim:

$$\underline{x} = \underline{x}_e + \delta\underline{x}$$
$$\underline{u} = \underline{u}_e + \delta\underline{u}$$

where subscript e denotes the reference trim or equilibrium state of the vehicle. Perturbations are assumed to be small such that terms involving products can be neglected, and a small angle approximation is adopted. The external forces, X , Y, Z, and moments L, M, N, are linearised through a Taylor expansion about the trim condition, where all except the first order terms are neglected. A fundamental premise behind Taylor's Theorem is that the forces and moments are analytic functions of the disturbed motion variables and their time derivatives. With this assumption, these functions can then be estimated from an expansion about any known point within the analytic range. The external force applied along the x-axis can therefore be expressed in approximate linear form as

$$X = X_e + X_u\delta u + X_w\delta w + \ldots + X_{\theta_{0tr}}\delta\theta_{0tr}$$

where $X_u = \dfrac{\partial X}{\partial u}$ etc are known as the stability and control derivatives. Similar expansions may be written down for the remaining forces and moments. Note that

terms in the rates of change of state and control variables with time (e.g. $\frac{\partial X}{\partial \dot{w}}$) have been ignored.

The linearised equations of motion can now be expressed in standard state space form as

$$\delta \underline{\dot{x}}(t) = \left(\frac{\partial \underline{F}}{\partial \underline{x}}\right)_{\underline{x}=\underline{x}_e} \delta \underline{x}(t) + \left(\frac{\partial \underline{F}}{\partial \underline{u}}\right)_{\underline{x}=\underline{x}_e} \delta \underline{u}(t) \tag{2.10}$$

or, dropping the perturbation notation (δ) and introducing the system and control matrices, $\boldsymbol{A}$ and $\boldsymbol{B}$,

$$\underline{\dot{x}}(t) = \boldsymbol{A}\underline{x}(t) + \boldsymbol{B}\underline{u}(t) \tag{2.11}$$

The system and control matrices are given in full in appendix 2.

The main effort in linearisation lies in the determination of the stability and control derivatives. Although it is often possible to derive exact values analytically for aircraft and simple helicopter models, in practice numerical techniques are more commonly used. Due to the complexity of the model, the approach adopted here was based on numerical differencing. Rather than calculating the derivatives explicitly, each entry in the system A matrix was calculated, thus providing a useful check on the verity of the solution when comparing the purely kinematic entries with their expected values. The Genisa algorithm was modified so that, in turn, each of the 11 states and 4 controls could be positively and then negatively perturbed from it's trim condition. For each set of states and controls, the nonlinear equations of motion were evaluated and the corresponding system and control matrix entries calculated by central differencing i.e.

$$\boldsymbol{A}(i,j) = \frac{\dot{x}_i\left(x_j + \delta x_j\right) - \dot{x}_i\left(x_j - \delta x_j\right)}{2\delta x_j} \quad i,j = 1,11$$

$$\boldsymbol{B}(i,k) = \frac{\dot{x}_i\left(u_k + \delta u_k\right) - \dot{x}_i\left(u_k - \delta u_k\right)}{2\delta u_k} \quad i = 1,11;\ k = 1,4$$

The choice of perturbation size warrants careful consideration as it can influence the derivative value and hence have a significant effect on predicted stability and response characteristics. In theory, a small perturbation is best, since the numerical derivatives will converge to their exact analytic values as the perturbation size reduces to zero. However, if there is any significant nonlinearity at the trim condition of interest, then the predicted derivative may be misleading, since it will only be valid for disturbed flight involving very small amplitude perturbations from trim. Another problem associated with small perturbations is numerical. If the function of interest is insensitive to small increments in a particular state or control, then rounding errors may occur. Hence larger perturbation values are generally preferred, provided they are still small enough to capture the dynamics of the system. In practice a value of $\delta x_i = 0.05(x_{e_i})$, corresponding to 5% of the trim value, was adopted for the perturbation size.

The A matrix entries calculated by Genisa / Hibrom v.2 were compared with those predicted by two established simulation models, HGS and RASCAL. Both models were developed at Glasgow but HGS is an actuator disc model while RASCAL uses an individual blade representation of the main rotor. There are significant variations between all three sets of data, particularly in the off-axis derivatives. The main on-axis derivatives, however, are generally consistent in sign and order of magnitude. See appendix 3 for a comparison of the on-axis derivatives at 60 knots.

3 Stability Analysis of the Lynx Using Linearised Hibrom

The stability of any dynamic system is obtained by consideration of its free (unforced) motion. From the linear equations of motion derived in section 2.2(iii), it follows that the free motion of a helicopter can be described by the nth order initial value problem:

$$\dot{\underline{x}} = \boldsymbol{A}\underline{x}, \quad \underline{x}(0) = \underline{x}_0; \tag{3.1}$$

with solution

$$\underline{x}(t) = \boldsymbol{W}\mathrm{diag}\left[\exp(\lambda_i t)\right]\boldsymbol{W}^{-1}\underline{x}_0. \tag{3.2}$$

The eigenvalues, $\lambda_i, \quad i = 1, n$, of the system A matrix satisfy the characteristic equation

$$det[\lambda \boldsymbol{I} - \boldsymbol{A}] = 0 \tag{3.3}$$

and the nxn matrix of eigenvectors, $\boldsymbol{W}$, are such that

$$A\underline{w}_i = \lambda_i \underline{w}_i \tag{3.4}$$

Substituting (3.4) into equation (3.2), the free motion is seen to consist of a linear combination of n independent natural modes

$$\underline{x}(t) = \sum_{i=1}^{n} (\underline{v}_i{}^T \underline{x}_0) \exp(\lambda_i t) \underline{w}_i ; \tag{3.5}$$

where $\underline{v}_i$ are the eigenvectors associated with the transpose of the system matrix, $\boldsymbol{A}^T$. The modes are described as linearly independent since no single mode can be reproduced from a linear combination of the others. The character of each mode; period, natural frequency, damping, time to half or double amplitude, is determined by the eigenvalue, while it's distribution among the n states is given by the eigenvector. The stability characteristics of a vehicle may be discussed in terms of the stability of each of its natural modes; a negative real part for each and every eigenvalue indicating dynamic stability. Figure 1 shows a root locus for the Lynx which is derived by plotting eigenvalues on the complex plane over a range of forward speeds, in this case from the hover up to 100 knots. The different modes are identified by their eigenvectors and, where necessary, by analysis of the 'uncoupled' longitudinal and lateral dynamics. Table 2 describes the characteristics of the system modes at a forward speed of 40 knots.

Mode	Eigenvalue	Natural Frequency ω_n (rad/sec)	Damping ζ	Period T (sec)	t_{half} or t_{double} (sec)
Roll	-7.54	-	-	-	0.09
Spiral	-0.38	-	-	-	1.81
Dutch Roll	-0.35±1.24i	1.29	0.27	5.07	1.96
Phugoid	0.07±0.49i	0.49	0.15	12.88	9.35
Pitch	-1.29	-	-	-	0.54
Heave	-0.65	-	-	-	1.07
Engine	-5.18	-	-	-	0.13
Engine	-2.34±2.64i	3.53	0.66	2.38	0.30

Table 2: Stability Characteristics of the Lynx @ 40 knots

The dynamic characteristics of an aircraft are traditionally considered in terms of longitudinal and lateral motion, as well as short and longer term behaviour. The helicopter modes of motion, however, are characterised by a high degree of coupling which makes this convenient distinction in most cases inappropriate. Nevertheless, six fuselage modes have been identified and can be loosely classified as the roll, spiral and dutch roll lateral modes and the phugoid, pitch and heave longitudinal modes. The roll, spiral, pitch and heave modes are stable and aperiodic, with strong coupling between the heave and spiral modes. The oscillatory dutch roll and phugoid are characterised by their natural frequency and damping, the phugoid being marginally unstable, but slow, with a time to double amplitude of around 9 seconds. The results are generally consistent with those expected of this type of helicopter[13]. In addition to the six fuselage modes there exist two engine modes corresponding to the rotorspeed and engine torque degrees of freedom. The engine dynamics will be considered in detail in the next chapter.

4. Generic Inverse Simulation Algorithm: Genisa

4.1 Review of Genisa v.1

The Genisa v.1 algorithm (version 1) proceeds by making an initial estimate of the applied control inputs which, over a predefined time increment, will move the helicopter to its desired location. These control displacements are then applied to the helicopter model and the equations of motion solved in the conventional manner (by numerical integration) to obtain the helicopter's states at the next time point. From these states, the actual position of the helicopter can be deduced and compared with the desired outcome. An iterative scheme is then set up whereby control displacements are adjusted until the error between desired and actual outputs is within a prescribed tolerance. This process is repeated for a series of time intervals yielding a control time history, $\underline{u}(t_k)$, for the complete manoeuvre, where:

$$0 \le t_k \le t_m, \quad 1 \le k \le n_{pts};$$

t_m is the time required to complete the manoeuvre and n_{pts} is the number of discrete points defining the manoeuvre.

The success of the method outlined above relies on the availability of a formal mathematical description of the specified manoeuvre[14]. For the hurdlehop manoeuvre considered in this report, the sixth order altitude profile given by:

$$z_e(t) = 64h\left[\left(\frac{t}{t_m}\right)^3 - 3\left(\frac{t}{t_m}\right)^2 + 3\left(\frac{t}{t_m}\right) - 1\right]\left(\frac{t}{t_m}\right)^3; \qquad (4.1)$$

where h is the height of the obstacle, has been found to be suitable. From this we obtain the desired output vector, $\underline{y}_{des}(t_k)$, which is expressed as a series of n_{pts} discrete points, equally spaced in time:

$$\underline{y}_{des}(t_k) = \left\{\ddot{x}_{e_{des}}(t_k) \quad \ddot{y}_{e_{des}}(t_k) \quad \ddot{z}_{e_{des}}(t_k) \quad \dot{\psi}_{des}(t_k)\right\}^T,$$

$$0 \le t_k \le t_m, \quad k = 1, n_{pts}.$$

This can be regarded as the input to the inverse simulation. Inertial accelerations are used instead of displacements to improve the stability of the solution[15] and heading, ψ, is normally constrained to zero for a longitudinal manoeuvre such as the hurdlehop. In addition, it is assumed that the manoeuvre is performed at constant velocity, V_f. The flow chart in Fig. 2 provides a more complete description of the solution procedure.

The integration approach to inverse simulation is computationally more intensive than its differentiation based counterpart. However, it does not suffer from the stability problems of numerical differentiation and it offers tremendous freedom with respect to modelling. Within the framework of an integration solution algorithm, it is possible to implement any model, including an individual blade model such as Hibrom. As discussed in section 2.1, many modelling assumptions were made to assist in the development of Hibrom v.1, including the assumption of constant rotorspeed. The necessity for this constraint is made clear when the nature of the rotor load calculations is considered. Rotor forcing is periodic, which means that the solution interval, Δt, must coincide with an integer number of main rotor periods (one quarter turn for the 4 bladed helicopter considered here). In adopting a constant rotorspeed and hence constant rotor period this time interval, which is required for definition of the manoeuvre, can be fixed throughout the simulation. The implication of a varying rotorspeed would be that the size of Δt must also vary, to match the main rotor period. This in turn implies that the manoeuvre flight path can no longer be established independently of the main algorithm.

The following section describes modifications which were made to the Genisa v.1 algorithm to enable the engine model described in 2.2 to be included in Hibrom.

4.2 Genisa with Rotorspeed Degree of Freedom

As discussed in section 4.1, the nature of the rotor forcing requires that the solution time interval matches an integer number of main rotor periods. Assuming constant rotorspeed, this interval is fixed throughout the simulation. The existing Genisa v.1 algorithm typically requires a time consistent with one half turn of the main rotor, which Rutherford[15] found to be "sufficiently long to allow the transient dynamics to settle". Once this discretisation interval has been established, the desired output can be calculated at each time point and used as input to Genisa v.1.

With the introduction of the rotorspeed degree of freedom, the period of the main rotor is no longer fixed and hence the solution interval must vary throughout the simulation. Consequently, the desired flight path can no longer be determined independently of the main program and the time required to complete the manoeuvre will not be known *a priori.*

This problem is overcome by expanding the control vector, $\underline{u}(t_k)$, to include an estimate of the next time point which will allow sufficient time for the rotor blades to sweep out the desired azimuth. The estimate is based on the value assigned to rotorspeed at the current time point. Similarly, the output vector, $\underline{y}(t_k)$, will now include blade azimuth. The augmented control and output vectors are then given by:

$$\underline{u}(t_k) = \left\{\theta_0(t_k) \quad \theta_{1s}(t_k) \quad \theta_{1c}(t_k) \quad \theta_{0tr}(t_k) \quad t_{k+1}\right\}^T$$

$$\underline{y}(t_k) = \left\{\ddot{x}_e(t_k) \quad \ddot{y}_e(t_k) \quad \ddot{z}_e(t_k) \quad \dot{\psi}(t_k) \quad \psi_{azi}(t_k)\right\}^T$$

The next time point, t_{k+1}, is determined such that the error between the actual and desired blade azimuth is minimised.

The desired output vector must now be calculated at each time point in turn and a subroutine for the hurdlehop has been written for this purpose. In due course, similar routines will be formulated to define other manoeuvres of interest such as the pop-up and slalom.

4.3 Verification of the Modified Genisa Algorithm

For verification purposes, a gentle hurdlehop manoeuvre is considered whereby the pilot's task is to clear a 5m high obstacle and return to the original altitude over a distance of 150m, whilst maintaining a constant forward speed of 40 knots. The obstacle is assumed to be located at the mid-point of the manoeuvre (Fig.3). Results will be compared directly with those obtained using the Genisa v.1 algorithm, which has itself undergone extensive verification[15]. It should be noted that, in each case, different initial trim conditions are used, since the revised version of Genisa (Genisa v.2) now trims with rotorspeed degree of freedom.

To ensure that the new algorithm has been implemented correctly, results are obtained first of all with the engine equations, (2.1) and (2.4), disabled. This means that the rotorspeed and engine states, Ω, Q_E, $\dot{Q}_E$, are held constant, isolating the operation of the new algorithm from any modifications made to the model. The results in Fig. 4 confirm that changes made to the existing Genisa v.1 algorithm have not affected the verity of the solution. Any discrepancy between the two sets of data may be attributed to the different starting conditions.

Figures 5 and 6 show time histories of the controls and engine states for the same manoeuvre with the full engine model implemented, again plotted against the Genisa v.1 result. In this case, a solution time interval corresponding to two turns of the main rotor has been used, $\Delta t_k = \frac{4\pi}{\Omega_k}$. Physically, a step input is made in each of the four controls which are then held constant over this period. The two sets of results are qualitatively similar, although the addition of an engine model with rotorspeed degree of freedom has clearly influenced the magnitude of the control displacements. The new Genisa v.2 inverse simulation predicts a greater range of control movements necessary to fly the specified manoeuvre and it may be expected that a greater difference between the two sets of results will be observed for more severe manoeuvres.

When the frequency of control application is increased to once per revolution of the main rotor the results deteriorate, with unstable oscillations developing in the lateral cyclic control and engine torque derivative as shown in Figs. 7 and 8. Furthermore, the simulation will not perform with a solution interval corresponding to one half turn of the rotor. However, with the engine model time constants, τ_{e1}, τ_{e2}, τ_{e3}, reduced to 1% of their nominal values, the results improve and a control application interval of once per revolution now produces smooth control time histories and engine states (Figs.9 and 10). This suggests that the control application interval must be carefully selected to accommodate the engine model dynamics.

4.4 Analysis of the Engine Dynamics

The dynamics of the engine model will now be studied analytically in order to explain the importance of the control application interval size. Assuming the engine torque derivatives, $\ddot{Q}_E$ and $\dot{Q}_E$, are relatively small and can be neglected, the 2nd order differential equation (2.4) describing the engine torque response to a change in rotorspeed simplifies to:

$$Q_E = K_3\left(\Omega - \Omega_i + \tau_2\dot{\Omega}\right) \tag{4.2}$$

Similarly, neglecting the fuselage yaw rate, $\dot{r}$, the equation relating rotor acceleration to applied torque becomes

$$\dot{\Omega} = \frac{1}{I_r + I_{tr}}\left(Q_E - Q_R - Q_{tr}\right) \tag{4.3}$$

Substituting equation (4.2) into (4.3) yields a first order differential equation in rotorspeed which can be written in standard form

$$\dot{\Omega}(t) + \left(\frac{-K_3}{I_R + I_{tr} - K_3\tau_2}\right)\Omega(t) = \frac{-K_3\Omega_i - Q_R - Q_{tr}}{I_R + I_{tr} - K_3\tau_2} \tag{4.4}$$

and has a solution of the form:

$$\Omega(t) = \frac{B}{A}\left(1 - e^{-At}\right),$$

where

$$A = \frac{-K_3}{I_R + I_{tr} - K_3\tau_2} \quad \text{and} \quad \frac{B}{A} = \frac{-K_3\Omega_i - Q_R - Q_{tr}}{I_R + I_{tr} - K_3\tau_2} \tag{4.5}$$

The time constant associated with this first order approximation to the engine dynamics is then

$$T = \frac{I_R + I_{tr} - K_3\tau_2}{-K_3} \tag{3.6}$$

Substituting data for the test configuration of the Westland Lynx;
$K_3 = -14414.3$, $I_R = 1714.948$, $I_{tr} = 324.0$, $\tau_2 = 0.256$ (average value at 40 knots):

$$T = 0.397 \text{ sec}.$$

Physically, this constant represents the time taken to reach 63% of the steady state and it can be compared with the control application intervals corresponding to one half, one and two turns of the main rotor:

$$\Delta t_{1/2} = 0.0878 \text{ sec}$$
$$\Delta t_1 = 0.1755 \text{ sec}$$
$$\Delta t_2 = 0.351 \text{ sec}$$

It seems reasonable to expect that a minimum interval of about 0.35 seconds will be required to allow the transient engine dynamics to settle down towards a new steady state following each application of the controls. Increasing the frequency of control activity beyond this has been shown to result in an unstable, often meaningless, solution. However the stability analysis described in chapter 3 revealed that the fuselage modes have times to half amplitude which are comparable to or even greater than the engine time constant derived above. This forces the question; why was a control interval corresponding to one half turn of the main rotor found to be sufficient before the inclusion of an engine model? The most likely explanation is that the fuselage dynamics are only weakly coupled to the main rotor, while an engine and rotorspeed governor will operate directly on the main rotor dynamics, thus playing a critical role.

5. Conclusions

The dynamics of an engine and rotorspeed governor have been successfully added to the individual blade rotor model, Hibrom. Linearisation of the new model has facilitated an analysis of the stability characteristics of a Westland Lynx; the first time such an analysis has been performed using Hibrom. The on-axis stability and control derivatives calculated by Hibrom v.2 agree fairly well with those predicted by two established rotor models, HGS and RASCAL. The process of linearisation has therefore provided further evidence of the physical validity of Hibrom.

A series of modifications have been made to the solution algorithm, Genisa, to accommodate the addition of rotorspeed degree of freedom to the main rotor. Through the necessity to match rotor periodicity, the control application interval is now recalculated iteratively at each time step. The new algorithm has been verified for a gentle hurdlehop manoeuvre and the effect of control application interval size

has been investigated. An interval corresponding to two turns of the main rotor has been found to be suitable.

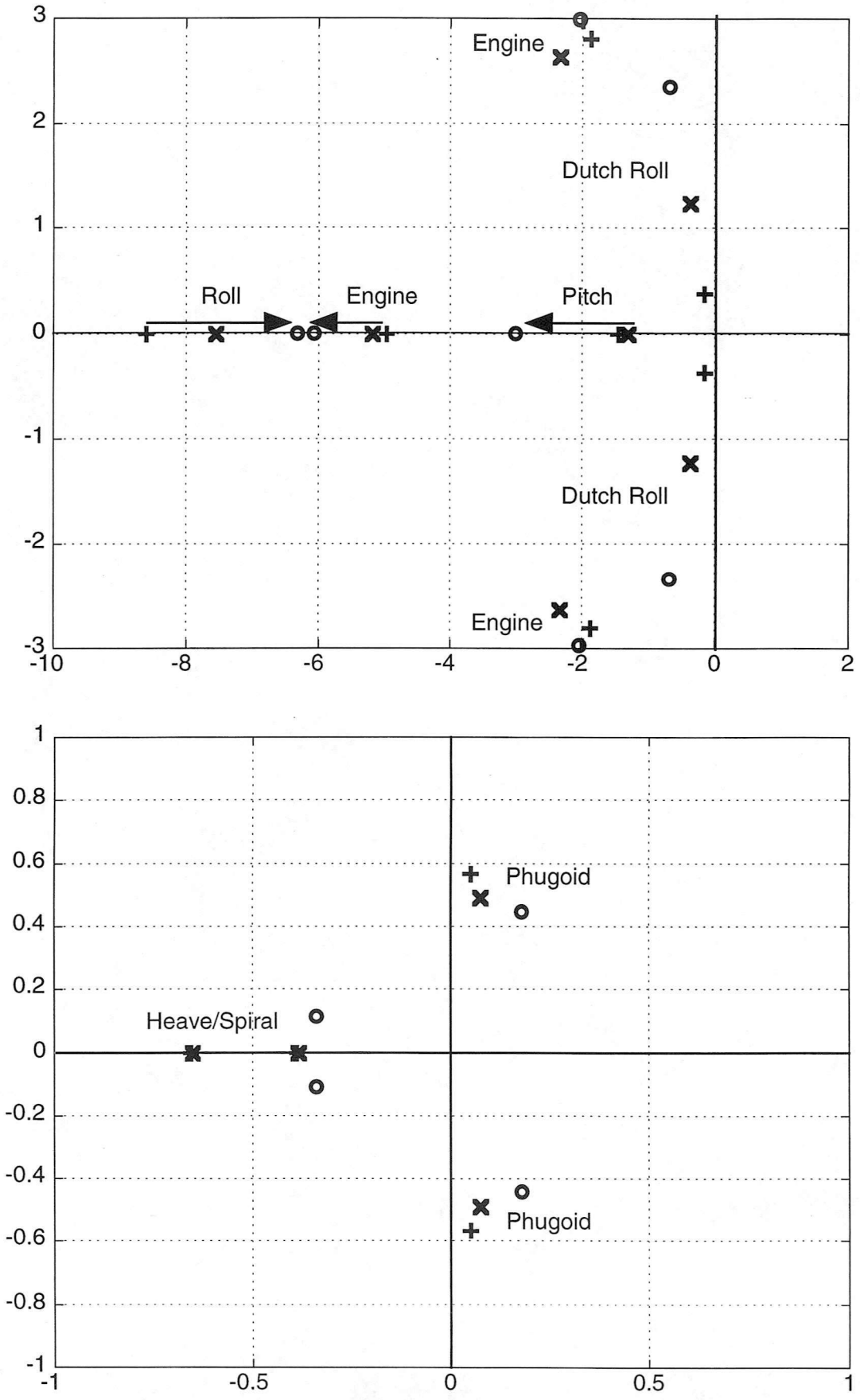

Figure 1 **Root locus plot of eigenvalues for the Lynx**

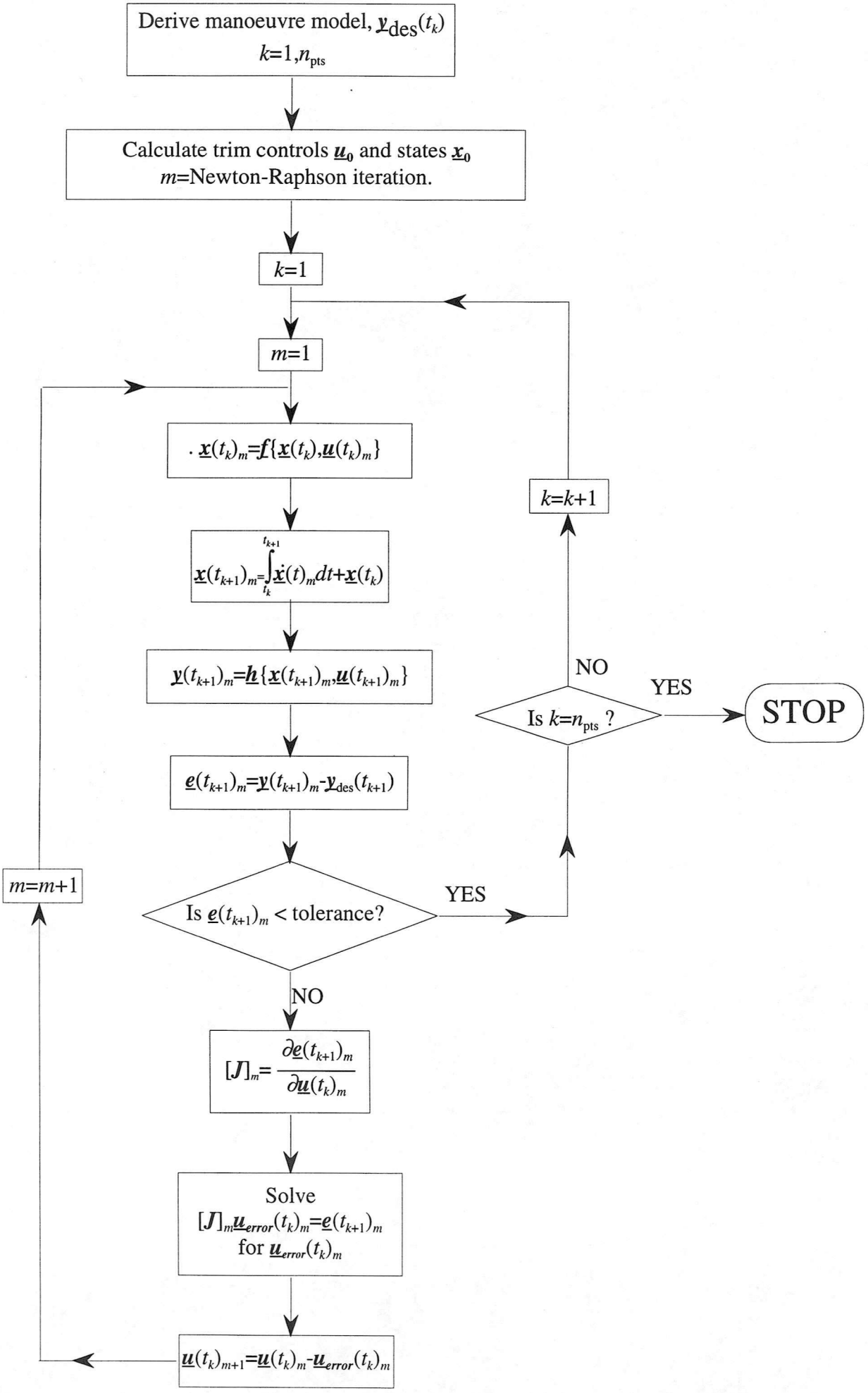

Figure 2 **Flowchart for the Genisa Algorithm**

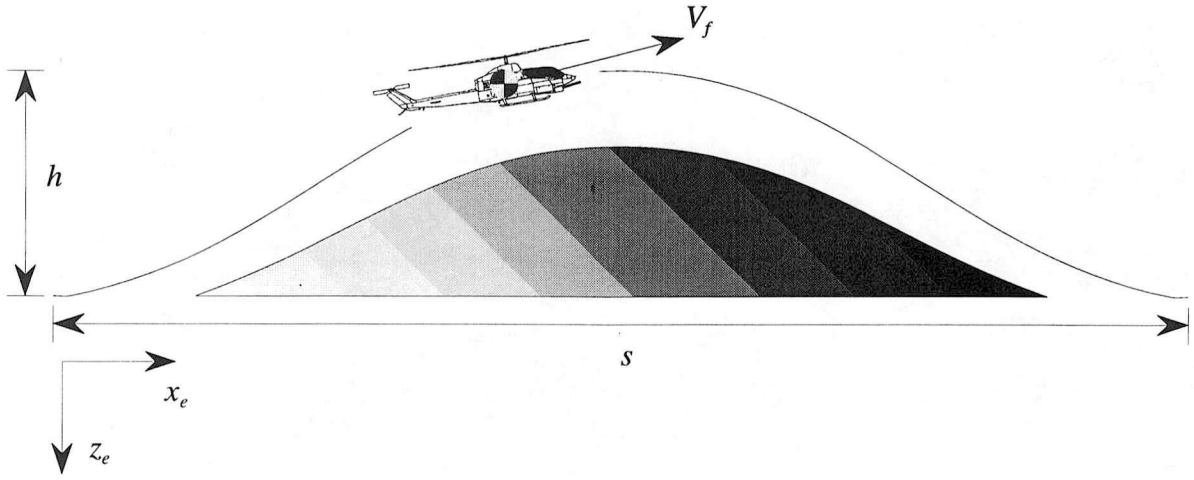

Figure 3 **The Hurdlehop Manoeuvre**

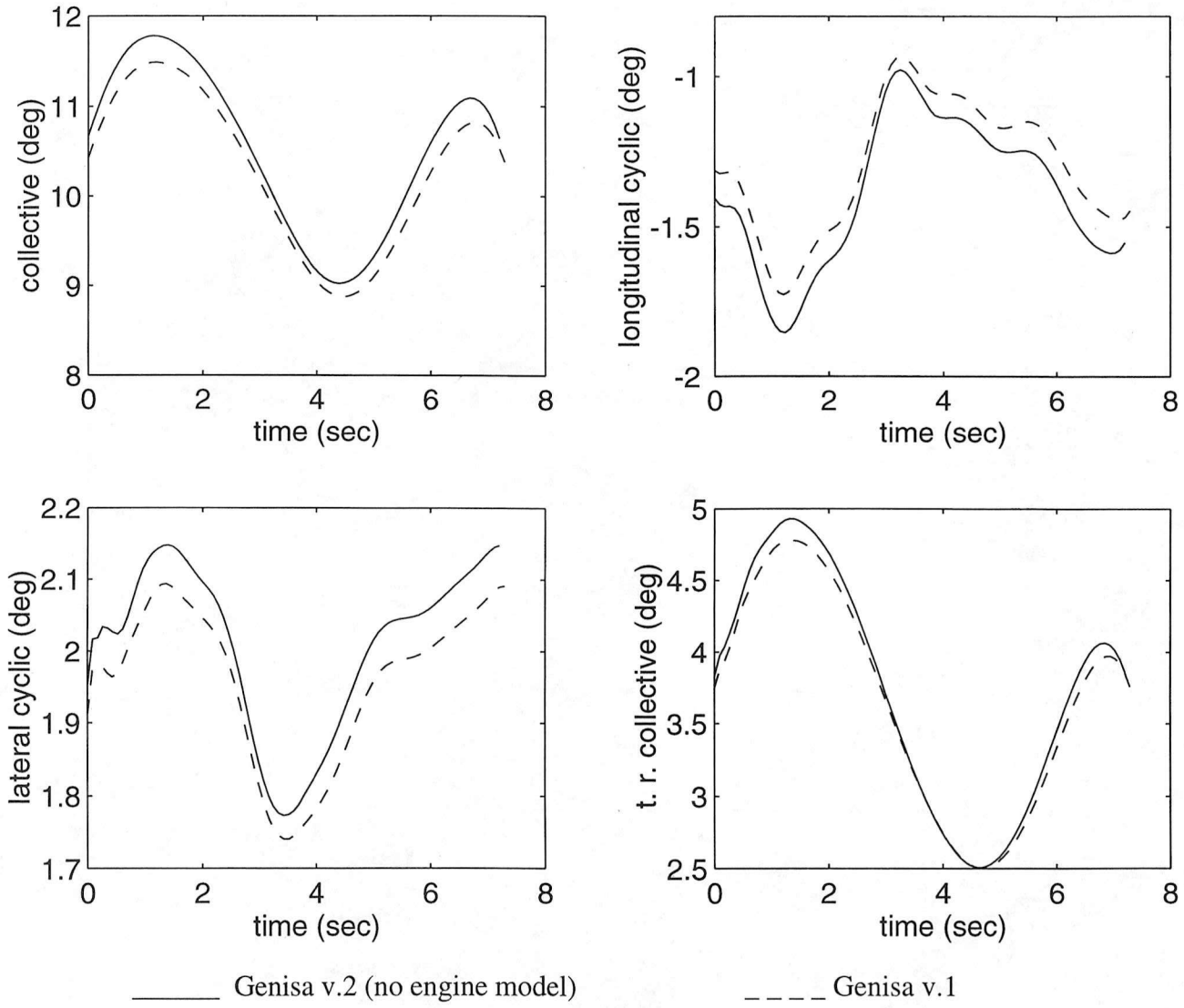

Figure 4 **Comparison between inverse simulation results generated by Genisa algorithms v.1 and v.2 (hurdlehop: V_f=40kts, h=5m, s=150m)**

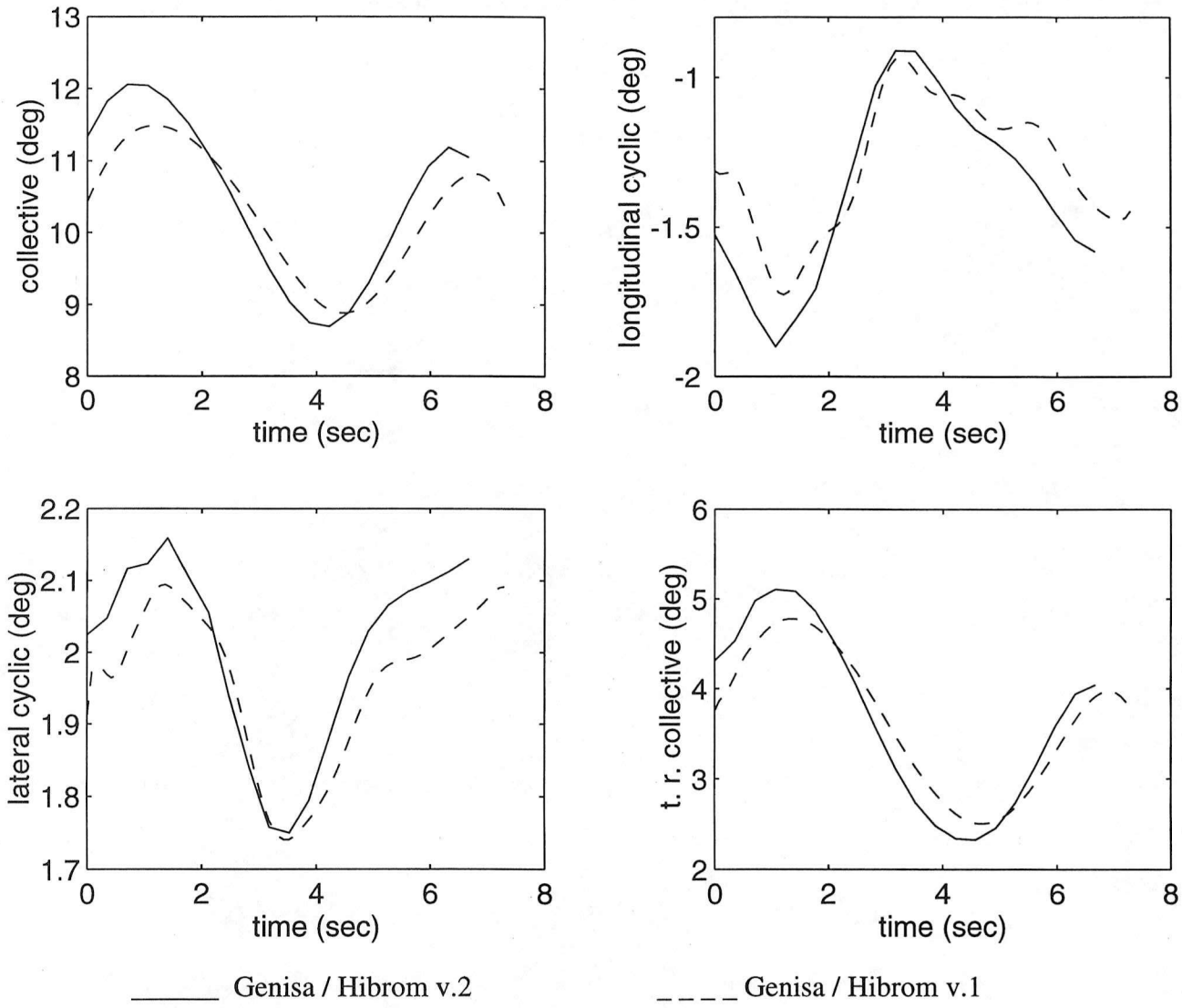

Figure 5 **Comparison between inverse simulation results generated by Genisa / Hibrom v.1 and v.2 (hurdlehop: V_f=40kts, h=5m, s=150m). Time step: 2 turns of main rotor**

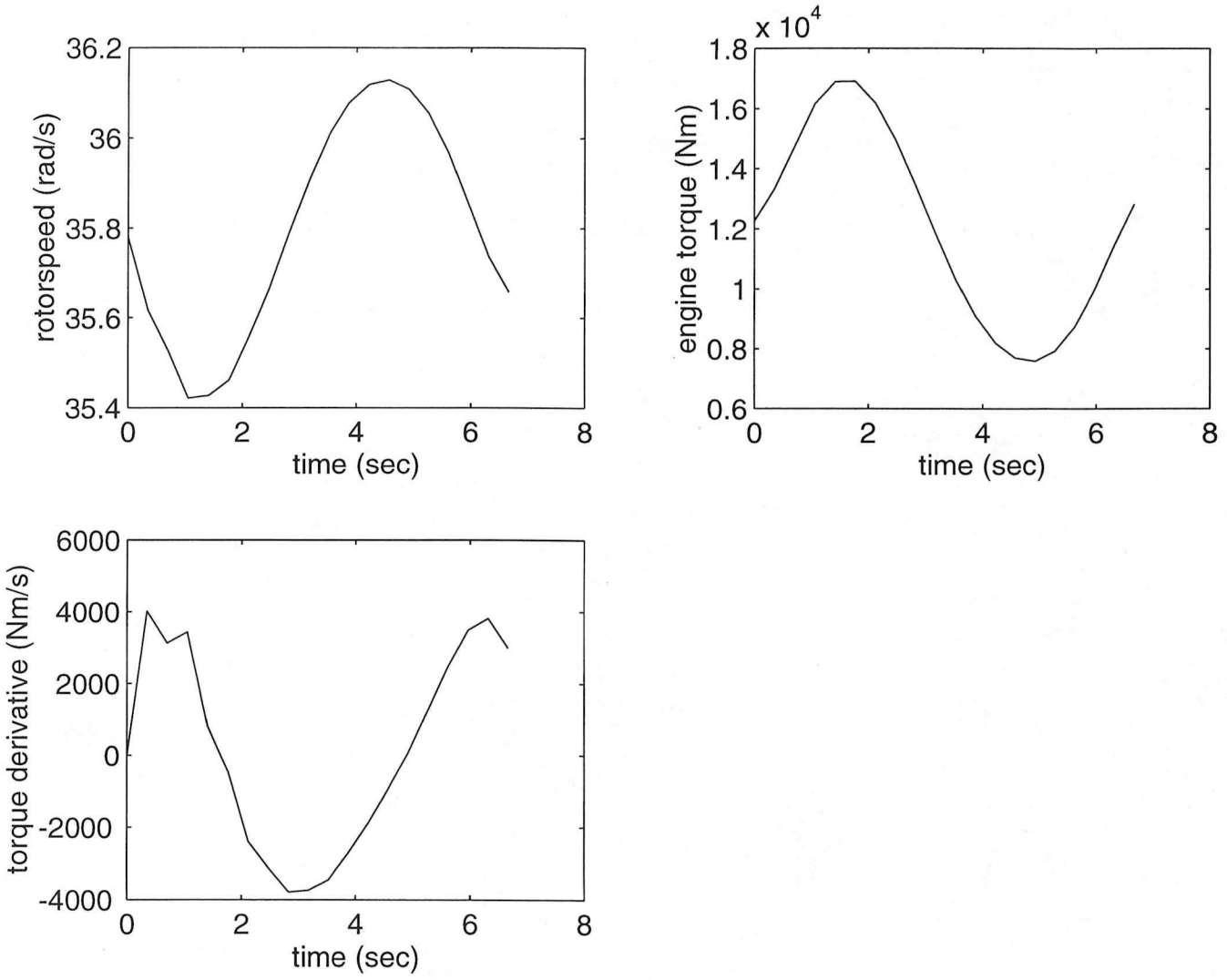

Figure 6 **Inverse simulation results generated by Genisa / Hibrom v.2 (hurdlehop: V_f=40kts, h=5m, s=150m). Time step: 2 turns of main rotor**

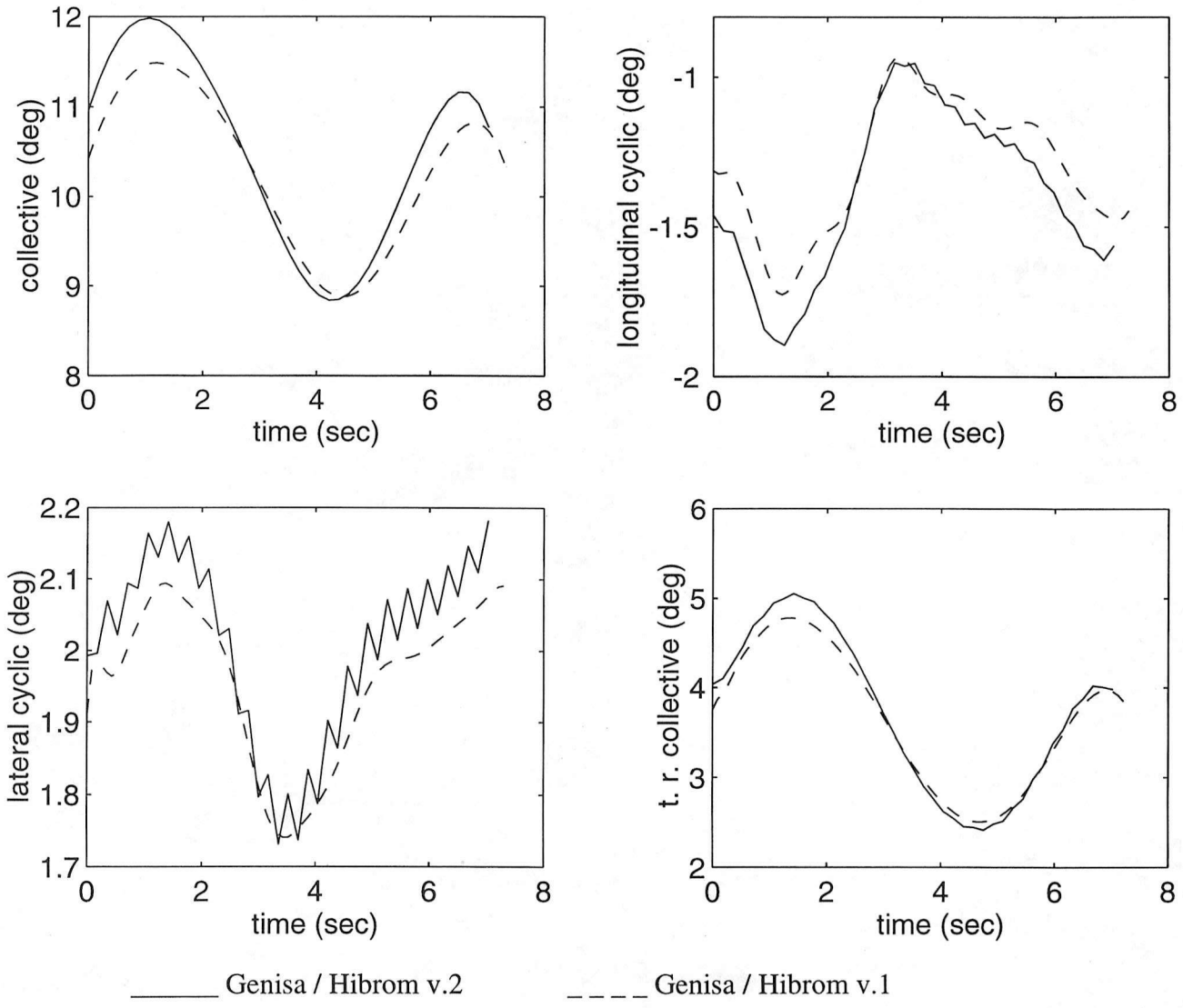

Figure 7 **Comparison between inverse simulation results generated by Genisa / Hibrom v.1 and v.2 (hurdlehop: V_f=40kts, h=5m, s=150m). Time step: 1 turn of main rotor**

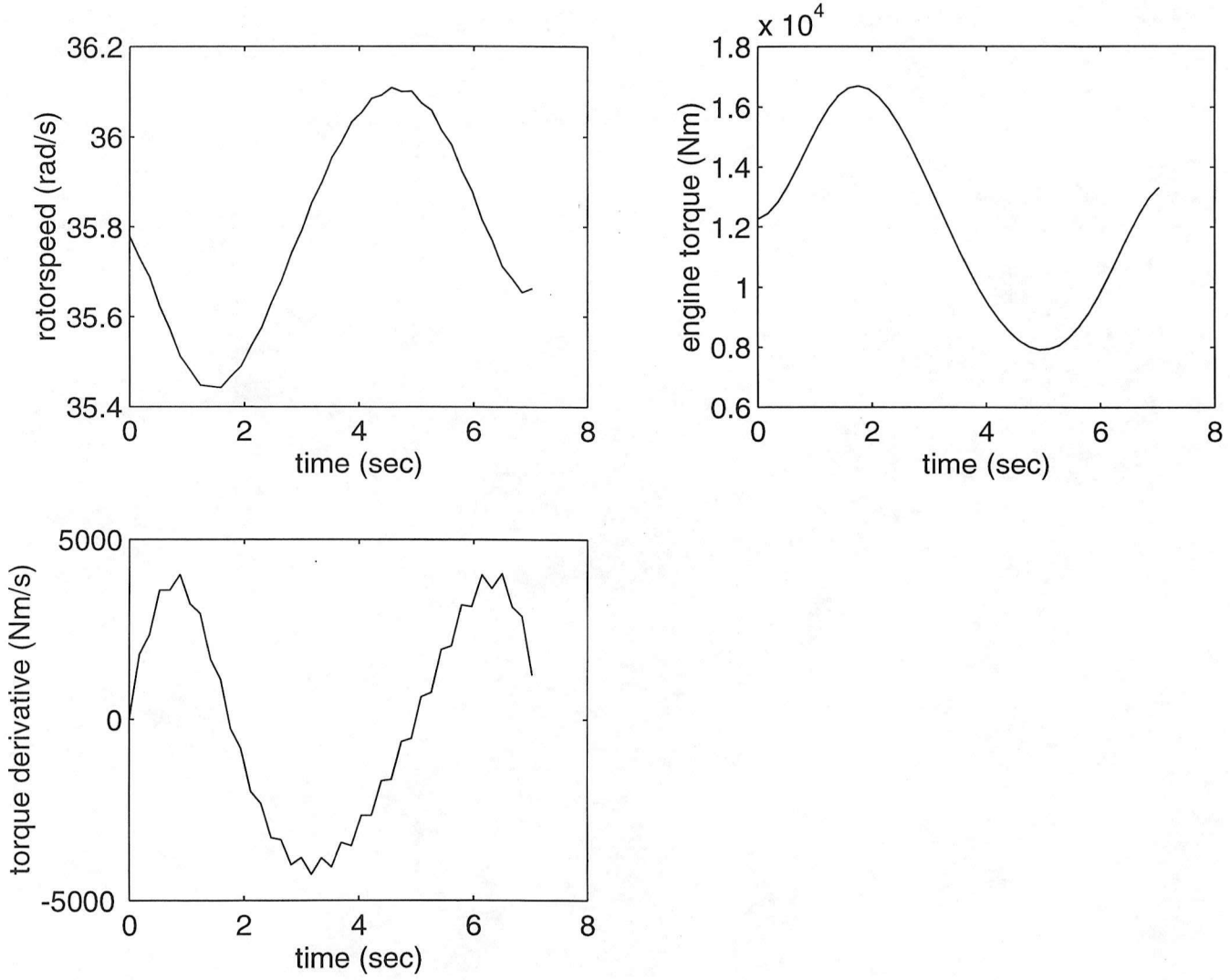

Figure 8 **Inverse simulation results generated by Genisa / Hibrom v.2 (hurdlehop: V_f=40kts, h=5m, s=150m). Time step: 1 turn of main rotor**

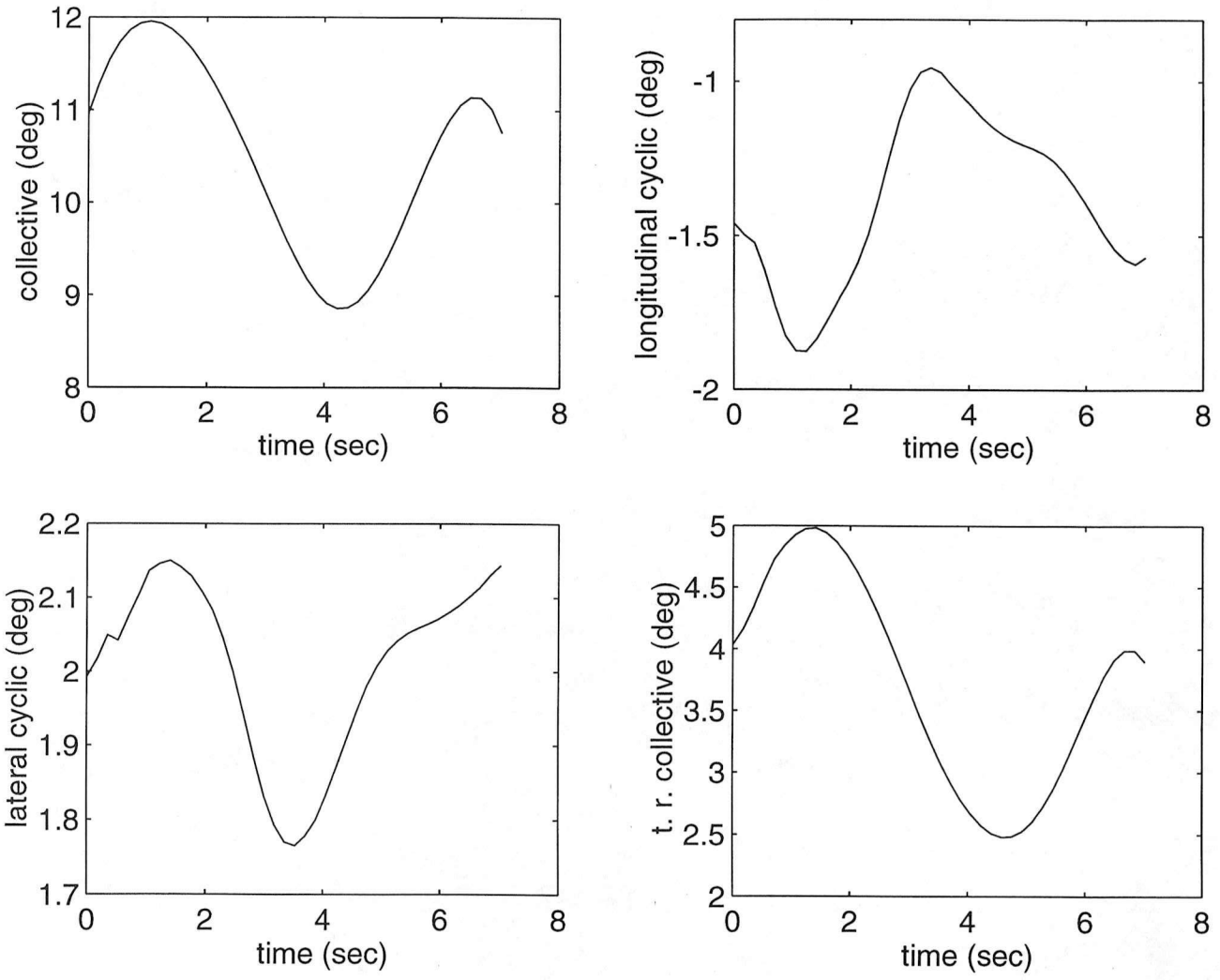

Figure 9 **Inverse simulation results generated by Genisa / Hibrom v.2 with low engine time constants (hurdlehop: V_f =40kts, h=5m, s=150m). Time step: 1 turn of main rotor**

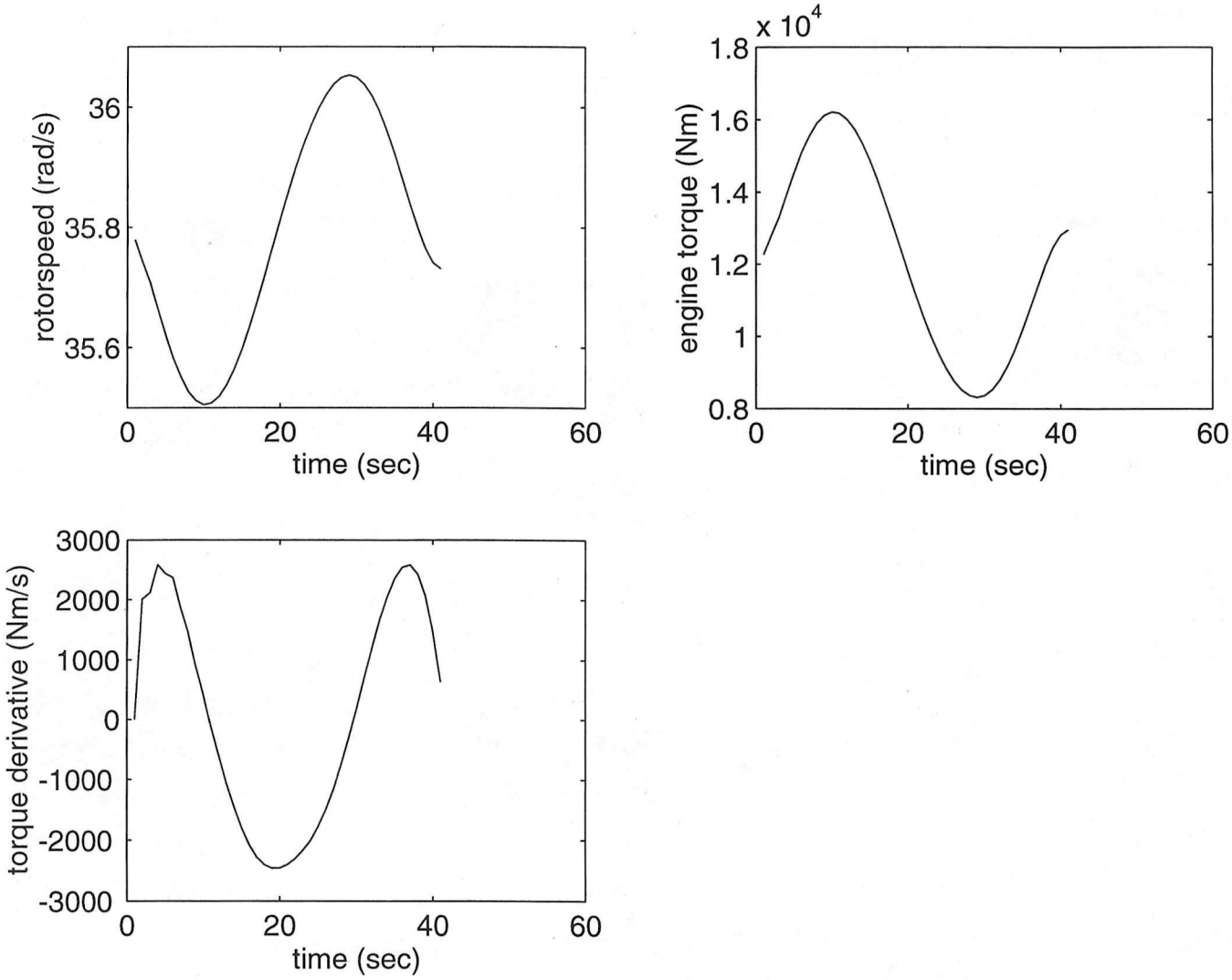

Figure 10 **Inverse simulation results generated by Genisa / Hibrom v.2 with low engine time constants (hurdlehop: V_f=40kts, h=5m, s=150m). Time step: 1 turn of main rotor**

Appendix 1 The Euler Rigid Body Equations of Motion

The motion of a rigid body can be described mathematically by the Euler equations of motion which are stated below.

$$\begin{aligned}
\dot{u} &= -(wq - vr) + \frac{X}{m} - g\sin\theta, \\
\dot{v} &= -(ur - wp) + \frac{Y}{m} + g\cos\theta\sin\phi, \\
\dot{w} &= -(vp - uq) + \frac{Z}{m} + g\cos\theta\cos\phi, \\
I_{xx}\dot{p} &= (I_{yy} - I_{zz})qr + I_{xz}(\dot{r} + pq) + L, \\
I_{yy}\dot{q} &= (I_{zz} - I_{xx})rp + I_{xz}(r^2 - p^2) + M, \\
I_{zz}\dot{r} &= (I_{xx} - I_{yy})pq + I_{xz}(\dot{p} + qr) + N.
\end{aligned} \tag{A1.1}$$

An additional three equations will be required to solve for the nine unknowns $(u, v, w, p, q, r, \phi, \theta, \psi)$. Kinematic equations relating the attitude angles ψ, θ and ϕ to the body axes rotational velocities p, q and r are given by

$$\begin{aligned}
\dot{\psi} &= q\sin\phi\sec\theta + r\cos\phi\sec\theta, \\
\dot{\theta} &= q\cos\phi - r\sin\phi, \\
\dot{\phi} &= p + q\sin\phi\tan\theta + r\cos\phi\tan\theta.
\end{aligned} \tag{A1.2}$$

where

u, v, w	are the components of translational velocity relative to the body-fixed axes system;
p, q, r	are the angular velocities of the body axes;
ψ, θ, ϕ	are the yaw, pitch and roll attitude angles, defining the orientation of the body axes relative to the earth;
m	is the total mass of the vehicle;
I_{xx}, I_{yy}, I_{zz}	are the moments of inertia of the vehicle about the body axes;
I_{xz}	is the product of inertia of the vehicle;

X, Y, Z	are the external forces and moments acting in the three
L, M, N	orthogonal body axes directions.

Appendix 2 Linearised System and Control Matrices

$A =$

$$
\begin{bmatrix}
X_u & X_w - q_e & X_q - w_e & -g\cos\theta_e & X_v + r_e & X_p & 0 & X_r + v_e & X_\Omega & X_{\dot{Q}_E} & X_{Q_E} \\
Z_u + q_e & Z_w & Z_q + u_e & -g\cos\phi_e \sin\theta_e & Z_v - p_e & Z_p - v_e & -g\sin\phi_e \cos\theta_e & Z_r & Z_\Omega & Z_{\dot{Q}_E} & Z_{Q_E} \\
M_u & M_w & M_q & 0 & M_v & \begin{matrix} M_p - 2p_e\left(I_{xz}/I_{yy}\right) \\ -r_e\left(I_{xx} - I_{zz}\right)/I_{yy} \end{matrix} & 0 & \begin{matrix} M_r + 2r_e\left(I_{xz}/I_{yy}\right) \\ -p_e\left(I_{xx} - I_{zz}\right)/I_{yy} \end{matrix} & M_\Omega & M_{\dot{Q}_E} & M_{Q_E} \\
0 & 0 & \cos\phi_e & 0 & 0 & 0 & 0 & -\sin\phi_e & \dot{\theta}_\Omega & \dot{\theta}_{\dot{Q}_E} & \dot{\theta}_{Q_E} \\
Y_u - r_e & Y_w + p_e & Y_q & -g\sin\phi_e \sin\theta_e & Y_v & Y_p + w_e & g\cos\phi_e \cos\theta_e & Y_r - u_e & Y_\Omega & Y_{\dot{Q}_E} & Y_{Q_E} \\
L'_u & L'_w & L'_q + c_1 p_e - c_2 r_e & 0 & L'_v & L'_p + c_1 q_e & 0 & L'_r - c_2 q_e & L'_\Omega & L'_{\dot{Q}_E} & L'_{Q_E} \\
0 & 0 & \sin\phi_e \tan\theta_e & 0 & 0 & 1 & 0 & \cos\phi_e \tan\theta_e & \dot{\phi}_\Omega & \dot{\phi}_{\dot{Q}_E} & \dot{\phi}_{Q_E} \\
N'_u & N'_w & N'_q - c_1 r_e - c_3 p_e & 0 & N'_v & N'_p - c_3 q_e & 0 & N'_r - c_1 q_e & N'_\Omega & N'_{\dot{Q}_E} & N'_{Q_E} \\
\dot{\Omega}_u & \dot{\Omega}_w & \dot{\Omega}_q & \dot{\Omega}_\theta & \dot{\Omega}_v & \dot{\Omega}_p & \dot{\Omega}_\phi & \dot{\Omega}_r & \dot{\Omega}_\Omega & \dot{\Omega}_{\dot{Q}_E} & \dot{\Omega}_{Q_E} \\
\ddot{Q}_{Eu} & \ddot{Q}_{Ew} & \ddot{Q}_{Eq} & \ddot{Q}_{E\theta} & \ddot{Q}_{Ev} & \ddot{Q}_{Ep} & \ddot{Q}_{E\phi} & \ddot{Q}_{Er} & \ddot{Q}_{E\Omega} & \ddot{Q}_{E\dot{Q}_E} & \ddot{Q}_{EQ_E} \\
\dot{Q}_{Eu} & \dot{Q}_{Ew} & \dot{Q}_{Eq} & \dot{Q}_{E\theta} & \dot{Q}_{Ev} & \dot{Q}_{Ep} & \dot{Q}_{E\phi} & \dot{Q}_{Er} & \dot{Q}_{E\Omega} & \dot{Q}_{E\dot{Q}_E} & \dot{Q}_{EQ_E}
\end{bmatrix}
$$

$$\boldsymbol{B} = \begin{bmatrix} X_{\theta_0} & X_{\theta_{1s}} & X_{\theta_{1c}} & X_{\theta_{0tr}} \\ Z_{\theta_0} & Z_{\theta_{1s}} & Z_{\theta_{1c}} & Z_{\theta_{0tr}} \\ M_{\theta_0} & M_{\theta_{1s}} & M_{\theta_{1c}} & M_{\theta_{0tr}} \\ 0 & 0 & 0 & 0 \\ Y_{\theta_0} & Y_{\theta_{1s}} & Y_{\theta_{1c}} & Y_{\theta_{0tr}} \\ L'_{\theta_0} & L'_{\theta_{1s}} & L'_{\theta_{1c}} & L'_{\theta_{0tr}} \\ 0 & 0 & 0 & 0 \\ N'_{\theta_0} & N'_{\theta_{1s}} & N'_{\theta_{1c}} & N'_{\theta_{0tr}} \\ \dot{\Omega}_{\theta_0} & \dot{\Omega}_{\theta_{1s}} & \dot{\Omega}_{\theta_{1c}} & \dot{\Omega}_{\theta_{0tr}} \\ \ddot{Q}_{E\theta_0} & \ddot{Q}_{E\theta_{1s}} & \ddot{Q}_{E\theta_{1c}} & \ddot{Q}_{E\theta_{0tr}} \\ \dot{Q}_{E\theta_0} & \dot{Q}_{E\theta_{1s}} & \dot{Q}_{E\theta_{1c}} & \dot{Q}_{E\theta_{0tr}} \end{bmatrix}$$

where:

$$c_1 = \frac{I_{xz}\left(I_{zz} + I_{xx} - I_{yy}\right)}{I_{xx}I_{zz} - {I_{xz}}^2},$$

$$c_2 = \frac{I_{zz}\left(I_{zz} - I_{yy}\right) + {I_{xz}}^2}{I_{xx}I_{zz} - {I_{xz}}^2},$$

$$c_3 = \frac{I_{xx}\left(I_{yy} - I_{xx}\right) - {I_{xz}}^2}{I_{xx}I_{zz} - {I_{xz}}^2}$$

and

$$L'_p = \frac{I_{zz}}{I_{xx}I_{zz} - {I_{xz}}^2} L_p + \frac{I_{xz}}{I_{xx}I_{zz} - {I_{xz}}^2} N_p,$$

$$N'_r = \frac{I_{xz}}{I_{xx}I_{zz} - {I_{xz}}^2} L_r + \frac{I_{xx}}{I_{xx}I_{zz} - {I_{xz}}^2} N_r.$$

Appendix 3 Comparison of On-Axis Derivatives Calculated by Hibrom, HGS and RASCAL

The following two tables show the on-axis system and control matrix entries calculated at 60 knots by the three models; Hibrom, HGS and RASCAL.

System Matrix Entries	Hibrom	HGS	RASCAL
X_u	-0.032	-0.025	-0.031
$X_w - q_e$	0.039	0.032	0.01
$X_q - w_e$	-1.079	-0.895	-0.721
$Z_u + q_e$	0.040	-0.034	-0.041
Z_w	-0.777	-0.700	-0.667
$Z_q + u_e$	31.99	30.87	31.15
M_u	0.025	0.028	0.042
M_w	0.027	0.025	0.107
M_q	-1.36	-2.18	-1.92
Y_v	-0.125	-0.136	-0.112
$Y_p + w_e$	1.258	0.846	0.779
$Y_r - u_e$	-31.63	-30.48	-31.15
L'_v	-0.122	-0.170	-0.301
$L'_p + c_1 q_e$	-5.851	-10.52	-7.452
$L'_r - c_2 q_e$	-3.33	-0.968	0.227
N'_v	0.079	0.085	0.105
$N'_p - c_3 q_e$	-0.920	-1.98	0.654
$N'_r - c_1 q_e$	-0.144	-1.30	-0.933

Table A3.1: System matrix entries at 60 knots

Control Matrix Entries	Hibrom	HGS	RASCAL
X_{θ_0}	6.02	5.07	1.13
$X_{\theta_{1s}}$	-10.3	-8.80	-27.4
Z_{θ_0}	-128.5	-107.9	-103.0
$Z_{\theta_{1s}}$	-27.3	-21.0	-29.6
M_{θ_0}	11.18	10.32	27.2
$M_{\theta_{1s}}$	28.28	28.33	65.6
$Y_{\theta_{1c}}$	-5.35	-10.22	25.3
$Y_{\theta otr}$	6.66	6.49	4.96
$L'_{\theta_{1c}}$	-135.7	-157.6	326.0
$L'_{\theta otr}$	-0.35	-1.29	19.75
$N'_{\theta_{1c}}$	-21.08	-27.96	-29.78
$N'_{\theta otr}$	-15.03	-17.48	-17.70

Table A3.2: Control matrix entries at 60 knots

References

1. Gao, C. and Hess, R.A., "Inverse Simulation of Large-Amplitude Aircraft Maneuvers", *Journal of Guidance, Control, and Dynamics,* Vol. 16, No. 4, 1993, pp. 733-737.

2. Borri, M., Bottasso, C.L. and Montelaghi, F., "Numerical Approach to Inverse Flight Dynamics", *Journal of Guidance, Control, and Dynamics,* Vol. 20, No. 4, 1997, pp. 742-747.

3. Thomson, D.G., Talbot, N., Taylor, C., Bradley, R. and Ablett, R., "An investigation of piloting strategies for engine failures during take-off from offshore platforms", *Aeronautical Journal,* 99 (981) (1995) 15-25.

4. Thomson, D.G. and Bradley, R., "The Contribution of Inverse Simulation to the Assessment of Helicopter Handling Qualities", Paper 7.3.2, Proceedings of the 19th ICAS Conference, Anaheim, U.S.A., September 1994.

5. Leacock, G.R. and Thomson, D.G., "The Estimation of Helicopter Pilot Workload Using Inverse Simulation", University of Glasgow, Department of Aerospace Engineering, Internal Report No. 9624, September 1996.

6. Thomson, D.G., "Development of a Generic Helicopter Mathematical Model for Application to Inverse Simulation", University of Glasgow, Department of Aerospace Engineering, Internal Report No. 9216, June 1992.

7. Rutherford, S. and Thomson, D.G., "Improved Methodology for Inverse Simulation", *Aeronautical Journal,* Vol. 100, No. 993, 1996, pp. 79-86.

8. Rutherford, S. and Thomson, D.G., "Helicopter Inverse Simulation Incorporating an Individual Blade Rotor Model", *Journal of Aircraft,* Vol. 34, No. 5, September-October 1997.

9. Padfield, G.D., "A Theoretical Model of Helicopter Flight Mechanics for Application to Piloted Simulation", Royal Aircraft Establishment, Technical Report No. 81048, April 1981.

10. Young, M.I., "A Simplified Theory of Hingeless Rotors with Application to Tandem Helicopters", Proceedings of the 18th Annual National Forum of the American Helicopter Society, May 1962.

11. Thomson, D.G., "Development of a Generic Helicopter Mathematical Model for Application to Inverse Simulation", University of Glasgow, Department of Aerospace Engineering, Internal Report No. 9216, June 1992.

12. Houston, S., "Rotorcraft Aeromechanics Simulation for Control Analysis - Mathematical Model Definition", University of Glasgow, Department of Aerospace Engineering, Internal Report No. 9123, 1991.

13. Padfield, G.D., "Helicopter Flight Dynamics - The Theory and Application of Flying Qualities and Simulation Modelling", Blackwell Science 1996.

14. Thomson, D.G. and Bradley, R., "Mathematical Definition of Helicopter Maneuvers", *Journal of the American Helicopter Society,* October 1997.

15. Rutherford, S. "Simulation Techniques for the Study of the Manoeuvring of Advanced Rotorcraft Configurations", Ph.D. Dissertation, Department of Aerospace Engineering, University of Glasgow, March 1997.